

Decoupling the Impact of Entanglements and Mobility on the Failure Properties of Ultrathin Polymer Films

R. Kōnane Bay, Tianren Zhang, Shinichiro Shimomura, Mark Ilton, Keiji Tanaka, Robert A. Riggleman, and Alfred J. Crosby*



Cite This: *Macromolecules* 2022, 55, 8505–8513



Read Online

ACCESS |



Metrics & More

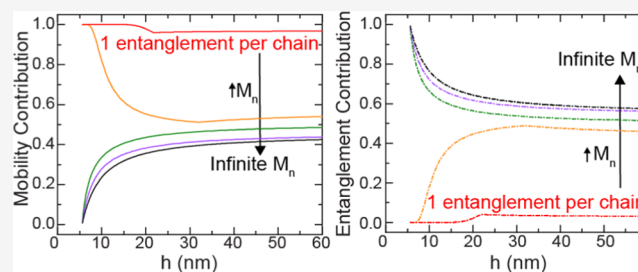


Article Recommendations



Supporting Information

ABSTRACT: The mechanical properties of glassy polymer thin films change as film thickness decreases below the average polymer molecule size. These changes have been associated with a reduction in interchain entanglements due to confinement and an increase in molecular mobility from the mobile surface layer. Here, using experiments and simulations, we determine how entanglements and surface mobility each individually impact the failure behavior of a glassy polymer film as the film becomes confined. We utilize a custom-built uniaxial tensile tester for ultrathin films and dark-field optical microscopy to characterize the complete stress–strain response and the associated strain localizations for ultrathin polystyrene films of varying thicknesses ($h = 10$ to 150 nm) for a range of molecular weights M_n of 61 to 2135 kDa. To directly correlate the changes in the molecular network to changes in the failure properties of ultrathin films, we perform nonequilibrium molecular dynamics simulations on $N = 250$, $N = 60$, with $h = 10$ to 30 nm. From our results, accounting for both the changes in entanglements and mobility, we propose a semiempirical model that captures the failure response in both simulated and experimental glassy polymer thin films.



INTRODUCTION

Glassy polymers thin films are ubiquitous in industrial applications, from flexible electronics to filtration membranes due to their ability to dissipate high stresses at low temperatures and flow at higher temperatures. However, in films with thicknesses below the average molecule size, polymers become extremely brittle, making ultrathin polymer films nearly unusable in many applications. Currently, to achieve mechanically robust ultrathin polymer films required for many technologies, an arbitrary minimum film thickness limit is selected. Thus, technological advancements for thin-film applications are hindered due to the lack of fundamental knowledge on how to rationally design mechanically stable ultrathin glassy polymer films.

In bulk glassy polymers, there are two primary effects that impact their mechanical strength and stability: entanglements between chains and chain mobility.^{1–13} For entanglements, the chain stiffness, contour length, and number average molecular weight, M_n , determine the nature of the entanglement network.¹¹ Previously, Mikos and Peppas developed a scaling linking the nature of the entanglement network to strength and toughness of polymer glasses.¹⁴ For polydisperse polymers, they predicted the strength and toughness scales $\exp(-2M_e/M_n)$, where M_e is the chain length between entanglements. In essence, the scaling suggests that below a critical molecular weight, there are more chain ends and fewer entanglements in the polymer network leading to a decrease in strength and

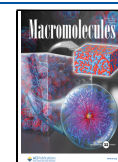
toughness. Recent work has extended this scaling to blends of short and long chains of glassy polymers in thin films with a fixed film thickness and showed that not all entanglements contribute to the mechanical integrity of the network.¹⁵ However, applying this scaling to homopolymer ultrathin films has yet to be explored due to the nature of the molecular entanglement network of ultrathin polymer films changing from the bulk state.

Specifically, in the ultrathin film state, when the film thickness decreases below the average configurational size of a polymer molecule, polymer chains at the boundary (surface) are reflected such that the polymer molecules at the interface become less entangled than the bulk molecules.^{16,17} This change suggests that at a critical film thickness, there is a reduction in interchain entanglements. Previous simulations have confirmed that the number of entanglements decreases and the entanglement molecular weight increases in the ultrathin state.^{18,19} From experiments, researchers have inferred a larger magnitude reduction in the number of entanglements compared to simulations.^{20,21} The loss of

Received: July 11, 2022

Revised: September 9, 2022

Published: September 27, 2022



strength and toughness in ultrathin polymer glasses has been previously associated with thickness-induced changes in entanglements.^{22–25} However, there is lack of agreement between simulations and experiments at what film thickness the reduction in entanglements is high enough to impact the mechanical strength. Therefore, an open question that remains is at what film thickness does the loss in mechanical integrity in the ultrathin state occur.

Additionally, chain mobility has been shown to affect mechanical strength in classical bulk studies. It is well-known that the mechanical strength and toughness decreases as the temperature approaches the glass-transition temperature, T_g , such that segmental mobility increases.^{26–29} The relationship between mobility and mechanical strength further complicates the understanding of the decrease in mechanical integrity in the ultrathin state as the average molecular mobility can change as the film thickness decreases. At a free surface, for polystyrene (PS), the polymer molecules have a higher relative mobility than the bulk, and this increase is often measured as a depression in the glass-transition temperature.^{16,30–32} The impact of this increase in average molecular mobility on failure strength has been previously not addressed directly in past experimental studies on the mechanics of ultrathin polymer films.^{22,23,33–35} Therefore, knowledge-based strategies to increase the failure strength of ultrathin films have been limited by the lack of understanding of how both the decrease in entanglements and increase in average molecular mobility contribute to the changes in failure properties. As such, despite the growth of techniques to measure the mechanical properties of ultrathin polymer films, a model has yet to be developed that quantitatively predicts how the mechanical strength and toughness change as film thickness decreases.

To understand how thickness impacts the failure properties of ultrathin polymer films and to use this knowledge to develop a model, it is necessary to measure and simulate how mechanical properties change with decreasing thickness and molecular weight. We utilize the model system PS as it is well characterized both in the bulk and the ultrathin states. We directly measure the uniaxial stress–strain response using The Uniaxial Tensile Tester for UltraThin films (TUTTUT) and observe the in situ strain localization of PS thin films with thicknesses, h , of 10 to 150 nm and M_n of 61 to 2135 kDa, where M_e is 18.1 kDa.³⁶ We use nonequilibrium molecular dynamics (MD) simulations to directly correlate the changes in the molecular network to changes in the failure properties of ultrathin films with number of monomers, $N = 250$, $N = 60$, with $h = 10$ to 30, where the typical number of monomers between entanglements (N_e) is around 16. All simulation values are in reduced units scaled by mass, van der Waals energy, and size of the polymer monomer (methods provided in the Supporting Information). We develop strong direct experimental evidence that film thickness and number of entanglements per chain both control the embrittlement of ultrathin polymer films. From our results, we propose a semiempirical model that captures the role of both the entanglement reduction and increased mobility on the failure properties of glassy polymer thin films in both experiments and simulations. The model can be applied to determine the minimum molecular weight required to fabricate mechanically strong ultrathin glassy PS films for industrial applications.

RESULTS AND DISCUSSION

Thin-Film Experiments and Simulations. To decouple how thickness and molecular weight change the entanglement network, we examine how the experimentally measured mechanical response of three different molecular-weight PS films changes as the film thickness decreases. Representative experimental stress–strain curves for 127, 553, and 876 kDa PS are shown in Figures 1a, and S2. For all three molecular

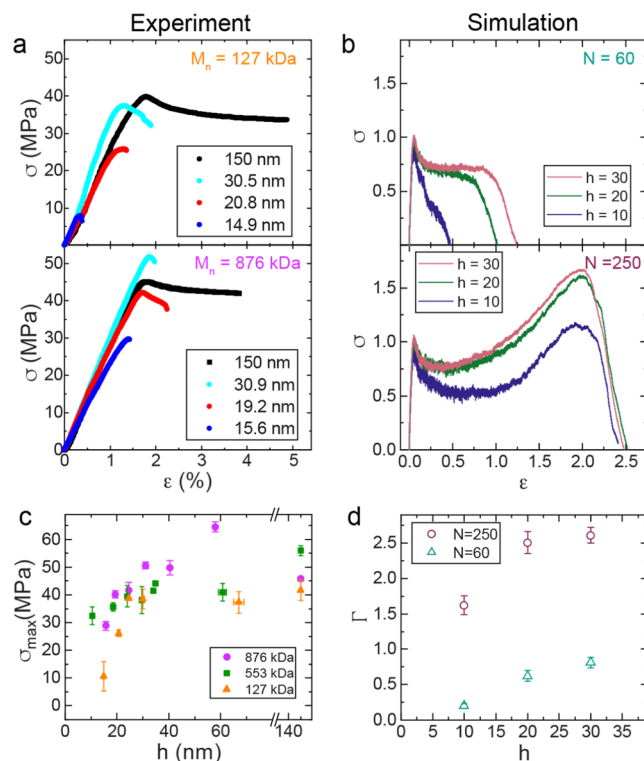


Figure 1. (a) Representative stress–strain response for 127 kDa (top) and 876 kDa (bottom) PS films with decreasing thicknesses measured experimentally. (b) Representative stress–strain response for $N = 60$ (top) and $N = 250$ at a simulated temperature of $T/T_g = 0.71$. (c) Maximum stress as a function of thickness, h for 876 kDa PS (pink circles), 553 kDa PS (green squares), and 127 kDa PS (orange triangles). Error bars represent five to seven individual films. The data for 127 kDa PS films (20 nm and thicker) are from ref 22. (d) Toughness as a function of thickness, h , for the simulated thin films of $N = 250$ (purple open circles) and $N = 60$ (teal open triangles).

weights, we observe an initial linear elastic stress–strain behavior followed by yield response. The yield stress and failure stress decrease as the film thickness decreases below a critical thickness, where the critical thickness depends on the molecular weight (Figures 1c and S3). For all three molecular weights of PS, the decrease in yield stress occurs as thickness decreases below ~ 30.0 nm.

Similar to experimental stress–strain responses, in the simulations we observe an initial linear elastic response for film thickness and molecular weights measured (Figure 1b). However, a more ductile response is observed at higher strains in the simulations.¹⁵ This discrepancy was recently addressed by Bukowski et al.,¹⁵ who demonstrated a quantitative link between changes in yield stress in the experiments to the toughness with varying entanglement networks, and the differences in ductility were rationalized through differences in the molecular friction and finite size effects in the

simulations. In the simulations, the measured toughness decreases as the film thickness decreases below $h = 20$, and $N = 250$ films are tougher than the $N = 60$ films at the same thicknesses (Figure 1d).

Additionally, we optically observe change in the failure mechanism as film thickness decreases for all three molecular weights (Figure 2a). The two failure mechanisms are crazing

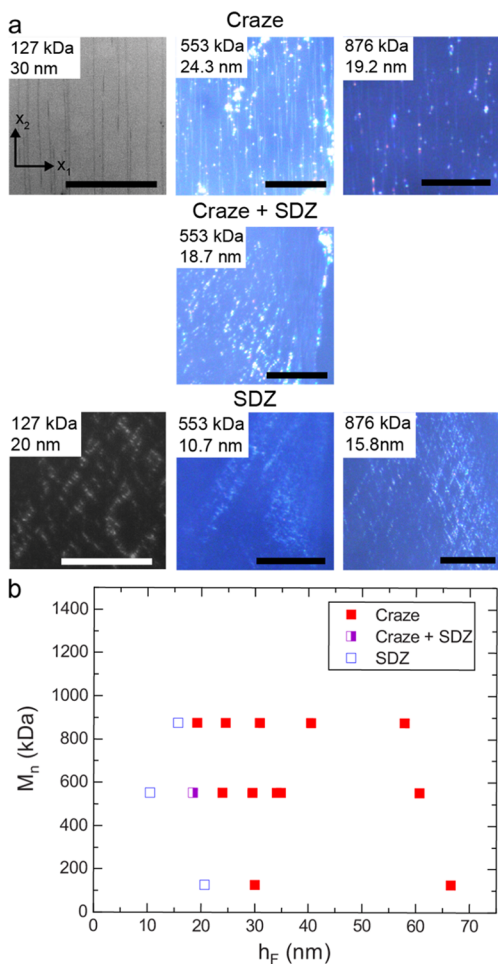


Figure 2. (a) Dark-field optical microscopy images of the films after failure for seven films (scale bars are $500 \mu\text{m}$). (Top row) crazes form in 30 nm thick 127 kDa PS, 24.3 nm thick 553 kDa PS, and 19.2 nm thick 876 kDa PS. (Middle row) mixture of craze and SDZs form in 18.7 nm thick 553 kDa PS. (Bottom row) SDZ form in 20 nm thick 127 kDa PS, 10.7 nm thick 553 kDa PS, and 15.8 nm thick 876 kDa PS. The 127 kDa 30 nm film image is inverted to enhance the contrast between craze and film. Both images of the 127 kDa films are reprinted in part with permission from *Macromolecules* 2018, 51, 10, 3657–3653. Copyright 2018 American Chemical Society. (b) Phase diagram as function of film thickness h and number average molecular weight M_n . Red filled squares are film thicknesses where crazes form. Blue open squares are the film thicknesses where SDZs form. Purple squares are the film thicknesses where a mixture of crazes and SDZs form.

and shear deformation zones (SDZs). Crazes are nanofibrillated zones that are formed perpendicular to the primary stress direction, and SDZs are shear bands that are formed 45° to the primary stress direction. We observe a weak molecular weight dependence on the transition from crazes to SDZs (Figure 2a). To probe this weak molecular weight dependence of strain localization thickness transition, we identify the

thicknesses where SDZs and crazes form for each molecular weight (Figure 2b). For 30 nm thick films, all three molecular weights of PS exhibit crazing. Through decreasing the thickness by 10 nm, we detect a molecular dependence on the strain localization morphology. At $\sim 19 \pm 1$ nm thick films, we observe only crazes for 876 kDa PS, mixtures of crazes and SDZ for 553 kDa PS, and only SDZ for 127 kDa PS. Below 19 nm, we observe only SDZ in 876 and 553 kDa at 15 and 10.5 nm, respectively. The thickness transition from crazing to SDZ has been previously associated with an increase in average molecular mobility from the mobile surface layer.²² The mobile surface layer has a higher chain mobility than the inner bulk layer.^{16,30–32} Thus, as the film thickness decreases, the volume fraction of the mobile surface layer in the film increases, leading to an increase in average mobility within the film. The increase in molecular mobility is often measured as a depression in the glass-transition temperature (T_g), which is decoupled from the confinement of a polymer film and is independent of molecular weight for substrate-supported PS.³⁷ However, we observe the transition from crazing to SDZ in thinner films as molecular weight increases, suggesting that the entanglement network could be playing a role.

Previous work has shown that changing the nature of the entanglement network can impact the yield and failure stress of glassy polymers.^{1–7,13} Researchers hypothesized that the drop in yield stress of the 127 kDa PS films has been associated with the loss of interchain entanglements as the film thickness decreased below the average polymer molecule size (radius end-to-end distance, R_{ee}), where the average polymer molecule size scales with molecular weight, $R_{ee} \sim M_n^{1/2}$.^{22,24} Thus, as molecular weight increases, the thickness at which the polymer becomes confined increases, suggesting that the drop in yield stress would be observed in thicker films at higher molecular weights. For all three molecular weights probed, critical thickness where the yield stress drop occurs is at similar thicknesses, $h < 25$ nm, which for 553 and 876 kDa PS is below their respective molecular sizes ($R_{ee} \sim 49$ and $R_{ee} \sim 61$ nm). Interestingly, the film thicknesses where we measure lower yield stress are at similar thickness where we observe SDZs, which indicates that the thickness-induced changes in molecular mobility are also impacting the yield and failure stress. In further support, previous studies on the bulk glassy PS have observed a decrease in yield and failure stress by increasing molecular mobility through increasing temperature.^{26–29}

Semiempirical Model. To understand the molecular weight and thickness dependence on the yield stress and toughness, we independently determine the impact of entanglements and mobility, by performing additional experiments on PS films at a fixed thickness with varying molecular weights and simulations on polymer films at a fixed thickness with varying temperatures. Furthermore, we review previous work on how strength and toughness in bulk glassy polymer change with the number of entanglements and mobility, and how entanglements and mobility change as a polymer film becomes confined. We show that a failure model that only accounts for changes in entanglements or mobility does not capture the results from the experiments and simulations. Therefore, we develop a semiempirical model that accounts for both the changes in entanglements and mobility.

First, to establish an independent baseline of the effect of number of entanglements per chain, $\langle Z \rangle = M_n/M_e$, on the failure properties of thin films, we experimentally measure the

stress–strain response of 150 nm thick PS films with molecular weights ranging from 61 to 2135 kDa (Figure S4). We observe a large drop in σ_{\max} as M_n decreases from 98 kDa PS to 61 kDa PS. We attribute this transition to a decrease in the number of entanglements per chain, $\langle Z \rangle$ from 5 to 3. Previous work suggested that a critical number of entanglements is necessary to form stable crazes in glassy polymer films.^{38,39} This drop in yield and failure stress has been previously observed near the same molecular weight for bulk PS.^{38,40} Kramer and co-workers also observed brittle behavior for $M_w < 58$ kDa in PS thin films ($h \sim 400$ nm).³⁹ Also, Mikos and Peppas established a model that captured how varying entanglement per chain through molecular weight impacts failure stress, $\sigma_f(M_n) = \sigma_{f,\infty} e^{(-2/\langle Z \rangle)}$ where $\sigma_{f,\infty}$ is the failure stress of a polymer with infinite long chains at a specific testing temperature.¹⁴ While this model works for changes in molecular weight, Bukowski, et al. found that it fails when the entanglement network is diluted through the blending short chains into long chains. They associated the lack of agreement between the Mikos and Peppas model and their results that not all of the entanglements in the entanglement network contribute to the load bearing network. Thus, they introduced the modified Mikos and Peppas model for yield stress, σ_{\max} and toughness, Γ to be

$$\frac{\sigma_{\max}}{\sigma_{\infty}} = \left(1 - \frac{\sigma_0}{\sigma_{\infty}}\right) e^{(-2/\langle Z_{\text{eff}} \rangle)} + \frac{\sigma_0}{\sigma_{\infty}} \quad \text{and}$$

$$\frac{\Gamma}{\Gamma_{\infty}} = \left(1 - \frac{\Gamma_0}{\Gamma_{\infty}}\right) e^{(-2/\langle Z_{\text{eff}} \rangle)} + \frac{\Gamma_0}{\Gamma_{\infty}}.$$

This model accounts for the yield stress and toughness both of infinitely long chains (σ_{∞} , Γ_{∞}) and assumes non-zero strength for short chains where no load bearing entanglements occur (σ_0 , Γ_0). Additionally, the entanglements counted in the model are the entanglements in the center of one chain whose partner is not a chain end, $\langle Z_{\text{eff}} \rangle$. In our bulk polymer films, we have only long chains and no short chain dilutants in our films, $\langle Z_{\text{eff}} \rangle = (\langle Z \rangle - 2)^2 / \langle Z \rangle$. Our results from our fixed thickness study are consistent with the modified Mikos and Peppas model (Figure S4).

However, applying the modified Mikos and Peppas model directly to films when the film thickness decreases below the average size of a polymer molecule becomes ill-defined due to the nature of the entanglement network being altered at these film thicknesses.^{18–21,30,41} Specifically, from the de Gennes and Silberberg scaling argument as a polymer becomes confined the polymer chains become more entangled with themselves (intra-chain entanglements) than that with neighboring chains (inter-chain entanglements).^{16,17} Decreasing inter-chain entanglements increases that entanglement molecular weight, M_e .^{20,30} The reduction in inter-chain entanglements and increase in entanglement molecular weight have been experimentally inferred, modeled, and simulated.^{18–20,30,41–44} From entanglement molecular weight that has been experimentally inferred, researchers have shown the change in entanglements with the confinement ratio, h/R_{ee} , where R_{ee} is the average size of a polymer molecule, R_{ee} .^{20,21} Here, we utilize the findings of Wang et al., who measured the disentanglement time to calculate entanglement molecular weight and found for PS thin films that entanglement molecular weight increases for the film thickness decreased below $h = 1.3R_{ee}$ for four different molecular weights.²¹ They empirically fit their data with a power law scaling and found $M_{e,\text{bulk}}/M_e(h) \sim (h/R_{ee})^{-0.86}$, when $h \leq 1.3 R_{ee}$

$$Z(h) = \frac{M_n}{M_e(h)} = \begin{cases} \frac{M_n}{M_{e,\text{bulk}}} \left[a \left(\frac{h}{R_{ee}} \right)^{-0.86} + b \right] & h \leq 1.3R_{ee} \\ \frac{M_n}{M_{e,\text{bulk}}} & h > 1.3R_{ee} \end{cases} \quad (1)$$

In our fitting, a and b are empirical constants calculated either from the empirical fit of the Wang et al. PS data for the experiments or from an empirical fit to the measured number of entanglements in the simulations (Figure S5). Using the empirical fit from the disentanglement times, we replot our experimental and simulation results as a function of the average number of entanglements in the system and compare them to the modified Mikos and Peppas model (Figure S6a,b).

If the entanglements were the only aspects impacting the change in the failure properties, the results would collapse onto a single curve. As shown in Figure S6a,b, we do not observe a collapse in the experimental or simulation data; thus, only accounting entanglements changing does not adequately describe the simulation or experimental results. This finding suggests that, unlike the previous hypothesis, the entanglement network being altered is not the only mechanism impacting the failure properties of thin films.

Beyond entanglements, strength and toughness are also dependent on the molecular mobility of the polymer. Explicitly, strength linearly decreases as molecular mobility increases.^{26–29} In the bulk, mobility can be increased by increasing the environmental temperature, T ,^{26–29} whereas in the ultrathin state, the average molecular mobility increases as film thickness decreases at a fixed temperature.^{16,30–32} We note that at low temperatures below the typical operating regime of glassy polymers ($T < 227$ K), the strength has been shown to plateau and become constant with decreasing temperature.²⁹

To establish the independent baseline on the impact of mobility on the failure of glassy polymers, we perform simulations on thin films with thicknesses of $h = 30$ and molecular weight of $N = 250$ at a range of temperatures, where the $T - T_g$ range is between -250 and 35 K (Figure S7). The simulations units here are converted to Kelvin for ease of comparison to experiments by multiplying by a factor of $\frac{T_{g,\text{bulk experiments}}}{T_{g,\text{bulk simulations}}} \sim 624$ K/reduced Lennard-Jones (LJ) units, where we assume the $T_{g,\text{bulk simulations}}$ in reduced LJ units measured from simulations is comparable to the $T_{g,\text{bulk experiments}}$ in real units measured for bulk PS. At $T - T_g < -100$ K, the toughness is constant as temperature decreases similar to strength measurements from previous experiments in the literature.²⁹ As the testing temperature increases, when $T - T_g > -100$ K, the toughness decreases linearly with temperature at temperatures less than glass-transition temperature, $T < T_g$, where previous models for failure and strength properties of bulk polymer glasses only accounted for entanglements and did not account for changes in mobility as it is constant at a fixed temperature in the bulk. However, in the thin-film case, mobility can change at fixed temperatures. In PS ultrathin films, the change in mobility is often measured and modeled as a depression in the T_g .^{37,45–51} For $T_g(h)$, previous work has developed an empirical relationship between the depression in T_g and film thickness expressed as

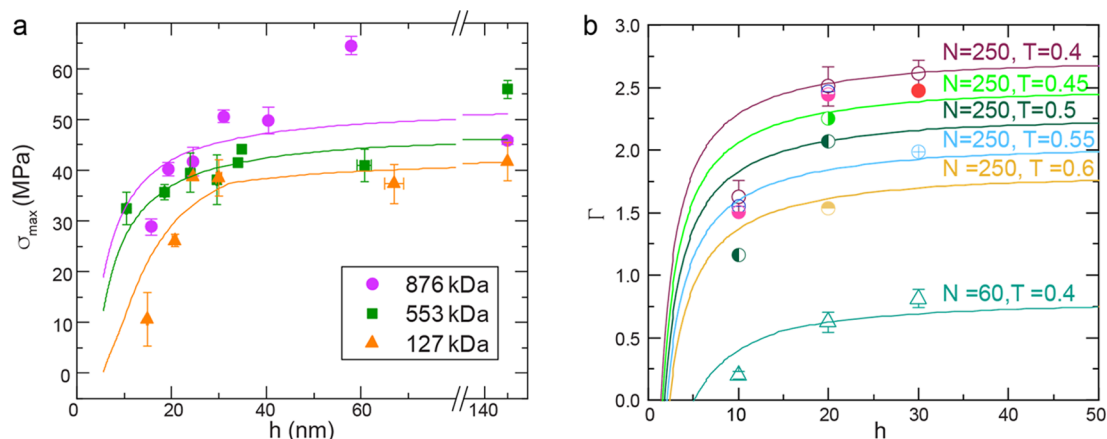


Figure 3. (a) Maximum stress as a function of thickness, h for 876 kDa PS (pink circles), 553 kDa PS (green squares), and 127 kDa PS (orange triangles) plotted with the semiempirical model (solid lines). (b) Toughness as a function of thickness, h for the simulated thin films of $N = 250$ (circles) and $N = 60$ (triangles) for different temperatures. The simulated thin films of $N = 60$ are measured at $T = 0.4$ (teal open triangles). The simulated films of $N = 250$ are measured at $T = 0.2$ (pink half circles), $T = 0.25$ (red half circle), $T = 0.3$ (dark blue open circle), $T = 0.4$ (open purple circles), $T = 0.45$ (lime green half circles), $T = 0.5$ (dark green half circle), $T = 0.55$ (light blue plus inscribed circles), and $T = 0.6$ (yellow half circles). The solid lines are the modified model for both the experiments and simulations for their associated data sets except simulated for $N = 250$ at $T = 0.2, 0.25,$ and 0.3 where the model is not valid.

$$T_g(h) = T_{g,\text{bulk}} \left(1 - \frac{c}{h}\right)^{1.8} \quad (2)$$

where $c = 3.2$ nm for supported PS films and $c = 7.8$ nm for freestanding PS films.^{37,51} To select a c value for experiments, we consider that the PS films are supported on a water surface. We use $c = 3.2$ for supported films as the thin films measured have one free surface and we do not know the impact of water on the surface mobility of PS. However, we do note that previous work has shown no difference in the yield stress between freestanding films and water-supported films.^{25,52} For simulations, we use $c = 0.9$, where the glass-transition temperature was quantified to calculate c . Using eq 2 to calculate $T_g(h)$, we replot the strength and toughness data as a function of $T - T_g(h)$. If the changes in mobility were only impacting the change in the failure properties, we expect the data would collapse on linear scaling from the bulk literature and our simulations at high molecular weight and thicknesses. However, similar to the above argument around entanglements, we did not observe a collapse onto a linear scaling. Thus, only accounting for mobility changing does not describe the failure properties of ultrathin films. Therefore, both the impact of mobility and entanglements need to be accounted for the changes in the failure properties.

Since neither changes in mobility nor changes in entanglements alone can capture the data, we further modify the Mikos and Peppas model to now account for the contribution in thickness-induced changes in both entanglements, $Z_{\text{eff}}(h)$, and mobility, $T_g(h)$ (eq 1). First, we account for how the long bearing chains $\langle Z_{\text{eff}} \rangle \rightarrow \langle Z_{\text{eff}}(h) \rangle$ changes with film thickness using eq 1, where $a = 0.702$ and $b = 0.456$ for experiments from the empirical fit of previous data, and $a = 0.1091$, $b = 0.924$ for the simulations from fitting to directly measured change in Z . Second, we allow both the maximum strength and toughness ($\sigma_{\infty}, \Gamma_{\infty}$) and single entanglement strength and toughness (σ_0, Γ_0) to be dependent on molecular mobility. From both previous literature data and our simulations, we expect both quantities to scale linearly as a function of $T - T_g(h)$. The modified model is given by

$$\sigma_{\text{max}}(M_n, h) = \alpha(T - T_g(h)) + \beta e^{(-2/\langle Z_{\text{eff}}(h) \rangle)} \quad (3)$$

for the experimental strength and

$$\Gamma(M_n, h) = \alpha(T - T_g(h)) + \beta e^{(-2/\langle Z_{\text{eff}}(h) \rangle)} \quad (4)$$

for the simulated toughness. Here, α is an empirical constant from a linear fit to the literature data and from our simulations performed at different temperatures where $\alpha = -0.31$ MPa/°C and $\alpha = -0.46$ (Figures S7 and S8). β is a fitting parameter calculated for each molecular weight, and the values are provided in Table S3. The thickness-dependent glass-transition temperature is calculated with eq 2. In Figure S9, we check the sensitivity of the model to the values of α , β , and c and find that the model is qualitatively the same though some tradeoffs between the three parameters. Figure 3a,b shows that both experimental and simulation data agree with the modified model. However, we do note that in the simulations at the lowest thickness, $h = 10$, the modified model does not fully capture the decrease in the toughness. Additionally, for the simulations, the model shows good agreement with varying the simulation temperature at $N = 250$.

The model provides an opportunity to decouple the influence of mobility and entanglements on the failure properties of ultrathin films. We calculate the relative contribution of the change in mobility, $\frac{\alpha(T - T_g(h))}{\sigma_{\text{max}}(M_n, h)}$ versus the change in entanglements, $\frac{\beta e^{(-2/\langle Z_{\text{eff}}(h) \rangle)}}{\sigma_{\text{max}}(M_n, h)}$ on the maximum stress with decreasing film thickness to evaluate their respective impact on the failure properties. We note that the model for maximum stress and toughness have same functional form, and previous work has shown that these properties can be compared; therefore, we only evaluate the relative contribution for yield stress.¹⁵

Before we discuss how mobility and entanglements individually contribute to yield stress and toughness, we consider how each affects the polymer chains as the chains undergo plastic deformation. We define the mobility contribution to plastic deformation as the amount of energy

required to move a polymer segment. Specifically, a polymer chain at a temperature below glass-transition temperature requires more energy to move a polymer segment compared to temperatures approaching the glass-transition temperature. In the thin film case, as film thickness decreases, the average polymer mobility increases; thus, the energy to move a polymer segment decreases. We define the entanglement contribution to plastic deformation as the amount of energy required to break or disentangle an entanglement between neighboring chains. This comes into play below a critical molecular-weight threshold, where the polymer chains have a small number of entanglements per chain, and the chains feel a larger force per entanglement and therefore require less energy to break or disentangle the chain. In the thin-film case, as film thickness decreases, the number of entanglements per chain decreases as a polymer film becomes confined, and accordingly, less energy is required to break a polymer chain in thinner films.

To decouple the role of mobility and entanglements on the energy to plastically deform ultrathin films, we examine the relative contribution of each for five molecular weights (Figure 4). For an infinitely high molecular weight as film thickness

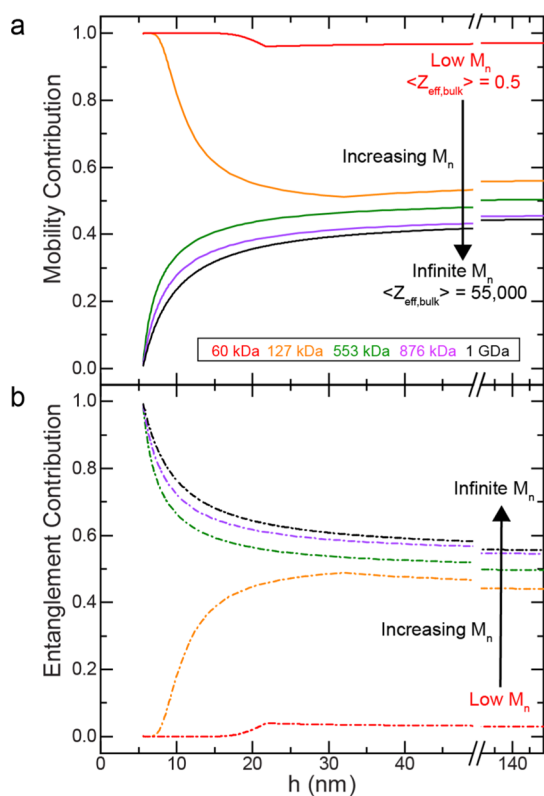


Figure 4. Decoupling the contribution of mobility and entanglements on the failure properties. (a) Relative contribution of (a) mobility and (b) entanglement contribution to the yield stress for five molecular weights.

decreases, the entanglement contribution to the yield stress increases while the mobility contribution decreases. We observe a similar trend for 876 and 553 kDa. For the lower molecular weight, 127 kDa, we observe the opposite trend; as film thickness decreases, the entanglement contribution decreases while the mobility contribution increases, which we associate with the low bulk number of entanglements per

chain, ~ 3.6 . In further support, at 60 kDa, where the bulk effective number of entanglements per chain is less than one, the mobility contributes more than the entanglements for all film thicknesses. We observe this lack of influence of entanglements on the failure properties in our experimental data for 150 nm thick 60 kDa films, where the yield stress is only ~ 10 MPa. This value is $\sim 20\%$ of the yield stress of 150 nm thick 876 kDa PS. The importance of chain mobility at low molecular weight is therefore expected since there are minimal entanglements in the system to provide network integrity.

Furthermore, we can apply the model to determine the minimum molecular weight to meet the design criteria for ultrathin glassy PS films used in industrial applications. For PS, we estimate by plotting the relative contributions of multiple molecular weights, the minimum molecular weight as a crossover molecular weight from where mobility dominates to where the entanglements provide the majority of the mechanical integrity as film thickness decreases to be ~ 200 kDa, where there are about eight entanglements per chain (details on the critical molecular-weight determination are provided in the Supporting Information). Below 200 kDa, we expect the loss of interchain entanglements due to the confinement to be large enough to lead to a loss of mechanical integrity. Above 200 kDa, the loss of interchain entanglements is not enough to lead to a loss in integrity, instead, the increase in molecular mobility from the mobile surface layers dominates and leads to the decrease. Thus, even at infinite molecular weights, the model suggests that there will always be a lower critical thickness limit, $h \sim 30$ nm (Figure S9), for single-component thin-film applications due to the increased molecular mobility, leading to the decrease in strength and toughness in ultrathin films.

Although our model provides an advance with regard to understanding the relative contributions from entanglements and molecular mobility to the mechanical response of ultrathin films, we acknowledge that many open questions remain, and further insight is required to provide a complete understanding of mechanical properties of polymer thin films. For example, our model does not directly account for polymer vitrification kinetics, strain rate, processing conditions, and simulation sample size.^{53–55} We additionally assume an average glass-transition temperature throughout the film and do not account for the inhomogeneity of the mobility within the film. Further development of models to account for such effects, as well as experimental and simulation studies to help guide and validate such models, will play an important role in continuing to refine the prescriptive engineering of polymer mechanical properties for a wide range of applications. Nonetheless, the insight provided by the model introduced here provides an important foundation for understanding the structure–property relationships that dictate the failure response of glassy polymer films.

Summary. In summary, using a combination of experiments and simulations, we measure how failure properties of glass polymer films change with molecular weight and film thickness. As film thickness decreases, we observe a molecular-weight-dependent decrease in maximum stress and toughness in both experiments and simulations, respectively. We systemically decouple the effect of the entanglements and mobility on the failure properties and find that both need to be accounted for when to be considered when designing the mechanically robust ultrathin glassy polymer films. To this end, we developed a model that can be used to determine the approximate molecular weight and thickness required to

fabricate mechanically strong ultrathin glassy polymer film for advanced polymeric applications.

EXPERIMENTAL METHOD

Materials. PS of seven different molecular weights were used: 61.9k PS (Polymer Source, number-average molecular weight, $M_n = 61.9$ kDa, PDI = 1.02), 98k PS (Scientific Polymer Products, $M_n = 98$ kDa, PDI = 1.04), 127k PS (Polymer Source, $M_n = 127$ kDa, PDI = 1.04), 235k PS (Polymer Source, $M_n = 235$ kg mol⁻¹, PDI = 1.07), 322k PS (Polymer Source, $M_n = 322$ kDa, PDI = 1.07), 553k PS (Polymer Source, $M_n = 553$ kDa, PDI = 1.07), 876k PS (Polymer Source, $M_n = 876$ kDa, PDI = 1.15), and 2136k PS (Polymer Source, $M_n = 2136$ kDa, PDI = 1.15). The 876k PS and 2136k PS were measured by light scattering. All other molecular weights were measured by gel permeation chromatography. The R_{ee} and average number of entanglements per chain (M_n/M_e) are provided in Table S1.

Sample Preparation. Thin-Film Fabrication. Toluene solutions of PS (0.2 to 2.5 wt %) were spun-cast (2000 to 4000 rpm) onto freshly cleaved mica sheet to fabricate the films with thicknesses from 10 to 150 nm.

Annealing Conditions. The films were annealed above the glass-transition temperature of PS and longer than the reptation time. Annealing conditions are listed in Table S2.

Laser Cutting. The films were laser-cut (Universal Laser System VSL3.5) at 3% power, 40% speed, and a setting of 800 PPI.

INSTRUMENTATION

TUTTUT. In brief, TUTTUT consists of a ‘dog-bone’-shaped film held between a reflective flexible cantilever and a movable rigid boundary on the liquid support layer of water. As the rigid boundary translates at a fixed velocity, the film stretches at a fixed strain rate and the cantilever deflects. The cantilever deflections are calibrated for force and displacement. Using the film geometry, we calculated the stress–strain response from the measured force displacement. We used dark-field optical microscopy to observe the deformation mechanisms in situ. We chose dark-field optical microscopy as it only images scattered light from the sample. Light scatters prominently from regions of the film with abrupt changes in optical density, which includes both the edges of the film and crazes and SDZs.

Loading Film into TUTTUT. Two methods were utilized to load the films into TUTTUT. For all molecular weights of the 150 nm thick and 60 nm thick PS films, the same method was used as in previous work.^{22,23} For the 30 nm and thinner 876 and 553 kDa PS, we changed the loading protocol due to folds forming in the gauge regime during the dropping of the clamp. For the second method, the films are floated off the mica substrate onto a water reservoir. The water level was lowered, and the grip section of the “dog-bone” was positioned into contact with a glass clamp coated with a PS film to promote adhesion between the “dog-bone” film and the clamp. The glass clamp was rigidly attached to the reservoir. The “dog-bone” was aligned with an extension piece attached to a cantilever, and the reservoir was raised to bring the other grip section of the “dog-bone” into contact with the extension piece.

Sample Geometry. For the first loading method, we utilized the same “dog-bone” geometry as chapter 2 where the gauge width was 3.1 mm. We measured the length between the grips (L_f) to calculate the gauge length, L_g using eq S1. For the second loading method, we changed the film geometry at the grip section. The new geometry is shown in Figure S1. The

gauge width was 3.1 mm, and we measured the L_f and calculated L_g by $L_g = (L_f - 17.5)^{0.96} + 16.4$.

In both methods, after the film was loaded into TUTTUT, the extra side material was picked up onto a silicon wafer for a thickness measurement. We measured the thickness of each PS film with ellipsometry (PS index of refraction, $n = 1.59$) and calculated the average from eight different locations on the same film.

Testing Conditions. The liquid in the reservoir was water. The length of the cantilever was changed to where the stiffness of the cantilever was three times the approximate stiffness of the film, which was calculated with eq S1. The stage velocity was fixed at 100 $\mu\text{m/s}$. Therefore, the 150 and 60 nm thick PS films were stretched at a strain rate between 6.1×10^{-3} and 6.9×10^{-3} s⁻¹, and 30 nm and thinner films were stretched at a strain rate between 5.6×10^{-3} and 6.1×10^{-3} s⁻¹ depending on the L_f of the film. The average temperature during the test was 21 °C.

Simulation Method. In the MD simulations, a modified version of the bead–spring Kremer–Grest (KG) model was shown,⁵⁶ where non-bonded interactions among monomers are taken through the LJ potential

$$U_{ij}^{\text{nb}} = 4\epsilon \left[\left(\frac{\sigma}{r} \right)^{12} - \left(\frac{\sigma}{r} \right)^6 \right] - 4\epsilon \left[\left(\frac{\sigma}{r_{\text{cut}}} \right)^{12} - \left(\frac{\sigma}{r_{\text{cut}}} \right)^6 \right]$$

for $r \leq r_{\text{cut}} = 2.5\sigma$. All the units are made dimensionless using the potential strength, ϵ , the monomer size, σ , and the unit time $\tau = \sigma(m/\epsilon)^{1/2}$, where m is the monomer mass. The bonded interactions between two connected monomers are governed by a finitely extensible nonlinear elastic potential with $k = 30\epsilon/\sigma^2$ and $R_0 = 1.5\sigma$. This bond type does not allow bond breaking during the uniaxial deformation process. We additionally add an angular harmonic potential

$$U_{\text{ang}} = \frac{K_\theta}{2} (\theta - \theta_0)^2$$

where $K_\theta = 10\epsilon/\text{radian}^2$ is the strength of this interaction and $\theta_0 = 120^\circ$ is the equilibrium bond angle. The angular potential is introduced to increase the average number of entanglements per chain without having very long polymer chain lengths, and the resulting average number of monomers between the entanglements is $\langle N_e \rangle \approx 16$. The number of monomers per chain in our simulations is $N = 60$, or 250, with $N/N_e = 3.75$ and 15.9, respectively. The polymer free-standing films with thickness of $H = 10\sigma$, 20σ and 30σ were generated following the procedures from our previous study,⁵⁷ but in this study, only homopolymer systems were considered. Once the free-standing films were constructed, three independent configurations of the films for each system were generated at high temperatures, and those polymer films were cooled from $T = 1.0 \left(\frac{T}{T_{g,\text{bulk}}} \approx 1.67 \right)$ to the target temperatures below $T_{g,\text{bulk}} \approx 0.598$ with a cooling rate of $\Delta T/\Delta t = 0.1$ per 2000τ to generate the glassy polymer thin films. Subsequently, each film was uniaxially deformed under a constant temperature at a constant true rate $\dot{\epsilon} = 1 \times 10^{-4}$ in the x -direction. Due to the extended simulation box in the z -direction, the samples were effective at constant pressure and can change volume during deformation by contracting in the z -direction. All the simulations are performed using LAMMPS MD simulation package with the velocity Verlet algorithm under an NVT

ensemble, and periodic boundary conditions were maintained in the plane of the film (x and y -directions) during all the simulations.⁵⁸

■ ASSOCIATED CONTENT

SI Supporting Information

The Supporting Information is available free of charge at <https://pubs.acs.org/doi/10.1021/acs.macromol.2c01435>.

Additional experimental details, 553 kDa stress–stress plot, failure stress as a function of thickness, experimental data for a fixed film thickness, simulation data on entanglements per chain, maximum stress and toughness plotted a function of entanglements and temperatures, literature data of failure stress plot versus temperature, sensitivity analysis of the model, and critical molecular-weight determination (PDF)

■ AUTHOR INFORMATION

Corresponding Author

Alfred J. Crosby – Polymer Science and Engineering,
University of Massachusetts, Amherst, Massachusetts 01003,
United States; Email: acrosby@umass.edu

Authors

R. Kōnane Bay – Polymer Science and Engineering, University
of Massachusetts, Amherst, Massachusetts 01003, United
States; Present Address: Department of Chemical and
Biological Engineering, University of Colorado Boulder,
Boulder, CO, USA; orcid.org/0000-0002-3980-8491

Tianren Zhang – Chemical and Biomolecular Engineering
Department, University of Pennsylvania, Philadelphia,
Pennsylvania 19104, United States; orcid.org/0000-0003-2899-5727

Shinichiro Shimomura – Polymer Science and Engineering,
University of Massachusetts, Amherst, Massachusetts 01003,
United States; Department of Applied Chemistry and Center
for Polymer Interface and Molecular Adhesion Science,
Kyushu University, Fukuoka 819-0395, Japan

Mark Ilton – Department of Physics, Harvey Mudd College,
Claremont, California 91711, United States

Keiji Tanaka – Department of Applied Chemistry and Center
for Polymer Interface and Molecular Adhesion Science,
Kyushu University, Fukuoka 819-0395, Japan; orcid.org/0000-0003-0314-3843

Robert A. Riggleman – Chemical and Biomolecular
Engineering Department, University of Pennsylvania,
Philadelphia, Pennsylvania 19104, United States;
orcid.org/0000-0002-5434-4787

Complete contact information is available at:
<https://pubs.acs.org/doi/10.1021/acs.macromol.2c01435>

Author Contributions

The manuscript was written through contributions of all authors. All authors have given approval to the final version of the manuscript.

Notes

The authors declare no competing financial interest.

■ ACKNOWLEDGMENTS

This work was financially supported from the National Science Foundation (NSF DMR 1608614, DMR 1904776, and DMR 1904525) and JST-Mirai Program (no. JPMJMI18A2). This

work used the Extreme Science and Engineering Discovery Environment (XSEDE), which is supported by the National Science Foundation grant number ACI-1548562.⁵⁹ This work used Stampede2 at the Texas Advanced Computing Center through allocation TG-DMR150034. R.K.B. acknowledges financial support from the University of Massachusetts Spaulding-Smith Fellowship. The authors also thank Cynthia Bukowski for helpful discussions.

■ REFERENCES

- (1) Bersted, B. H. Entanglement Network Model Relating Tensile Impact Strength and the Ductile brittle Transition to Molecular Structure in Amorphous Polymers. *J. Appl. Polym. Sci.* **1979**, *24*, 37–50.
- (2) Bersted, B. H.; Anderson, T. G. Influence of Molecular Weight and Molecular Weight Distribution on the Tensile Properties of Amorphous Polymers. *J. Appl. Polym. Sci.* **1990**, *39*, 499–514.
- (3) Zhao, Z.; Zhao, X.; Liu, J.; Wang, W.; Mays, J.; Wang, S. Q. Characterizing Effects of Fast Melt Deformation on Entangled Polymers in Their Glassy State. *J. Chem. Phys.* **2019**, *151*, 124906.
- (4) Razavi, M.; Cheng, S.; Huang, D.; Zhang, S.; Wang, S. Q. Crazing and Yielding in Glassy Polymers of High Molecular Weight. *Polymer* **2020**, *197*, 122445.
- (5) Wang, S.; Cheng, S.; Lin, P.; Li, X.; Wang, S.; Cheng, S.; Lin, P.; Li, X. A Phenomenological Molecular Model for Yielding and Brittle-Ductile Transition of Polymer Glasses. *J. Chem. Phys.* **2014**, *141*, 094905.
- (6) Donald, A. M.; Kramer, E. J. The Competition between Shear Deformation and Crazing in Glassy Polymers. *J. Mater. Sci.* **1982**, *17*, 1871–1879.
- (7) Turner, D. T. Tensile Strength Elevation of Brittle Polymers by Entanglements. *Polymer* **1982**, *23*, 626–629.
- (8) Watanabe, H.; Ishida, S.; Matsumiya, Y.; Inoue, T. Test of Full and Partial Tube Dilation Pictures in Entangled Blends of Linear Polyisoprenes. *Macromolecules* **2004**, *37*, 6619–6631.
- (9) Jackson, J. K.; Winter, H. H. Entanglement and Flow Behavior of Bidisperse Blends of Polystyrene and Polybutadiene. *Macromolecules* **1995**, *28*, 3146–3155.
- (10) Prest, W. M., Jr. Blending Laws for High-Molecular-Weight Polymer Melts. *Polym. J.* **1973**, *4*, 163–171.
- (11) Ferry, J. D. *Viscoelastic Properties of Polymers*, 3rd ed.; Wiley: New York, 1980.
- (12) Lin, P.; Xu, Q.; Cheng, S.; Li, X.; Zhao, Z.; Sun, S.; Peng, C.; Joy, A.; Wang, S. Q. Effects of Molecular Weight Reduction on Brittle-Ductile Transition and Elastic Yielding Due to Noninvasive Irradiation on Polymer Glasses. *Macromolecules* **2017**, *50*, 2447–2455.
- (13) Razavi, M.; Huang, D.; Liu, S.; Guo, H.; Wang, S. Q. Examining an Alternative Molecular Mechanism to Toughen Glassy Polymers. *Macromolecules* **2020**, *53*, 323–333.
- (14) Mikos, A. G.; Peppas, N. A. Polymer Chain Entanglements and Brittle Fracture. *J. Chem. Phys.* **1988**, *88*, 1337–1342.
- (15) Bukowski, C.; Zhang, T.; Riggleman, R. A.; Crosby, A. J. Load-Bearing Entanglements in Polymer Glasses. *Sci. Adv.* **2021**, *7*, No. eabg9763.
- (16) de Gennes, P. G. *Scaling Concepts in Polymer Physics*; Cornell University Press: Ithaca, NY, 1979.
- (17) Silberberg, A. Distribution of Conformations and Chain Ends near the Surface of a Melt of Linear Flexible Macromolecules. *J. Colloid Interface Sci.* **1982**, *90*, 86–91.
- (18) García, N. A.; Barrat, J. L. Entanglement Reduction Induced by Geometrical Confinement in Polymer Thin Films. *Macromolecules* **2018**, *51*, 9850–9860.
- (19) Sussman, D. M. Spatial Distribution of Entanglements in Thin Free-Standing Films. *Phys. Rev. E* **2016**, *94*, 012503.
- (20) Si, L.; Massa, M. V.; Dalnoki-Veress, K.; Brown, H. R.; Jones, R. A. L. Chain Entanglement in Thin Freestanding Polymer Films. *Phys. Rev. Lett.* **2005**, *94*, 127801.

- (21) Wang, F.; Jiang, Z.; Lin, X.; Zhang, C.; Tanaka, K.; Zuo, B.; Zhang, W.; Wang, X. Suppressed Chain Entanglement Induced by Thickness of Ultrathin Polystyrene Films. *Macromolecules* **2021**, *54*, 3735–3743.
- (22) Bay, R. K.; Shimomura, S.; Liu, Y.; Ilton, M.; Crosby, A. J. Confinement Effect on Strain Localizations in Glassy Polymer Films. *Macromolecules* **2018**, *51*, 3647–3653.
- (23) Choi, W. J.; Bay, R. K.; Crosby, A. J. Tensile Properties of Ultrathin Bisphenol-A Polycarbonate Films. *Macromolecules* **2019**, *52*, 7489–7494.
- (24) Liu, Y.; Chen, Y.-C.; Hutchens, S.; Lawrence, J.; Emrick, T.; Crosby, A. J. Directly Measuring the Complete Stress–Strain Response of Ultrathin Polymer Films. *Macromolecules* **2015**, *48*, 6534–6540.
- (25) Galuska, L. A.; Muckley, E. S.; Cao, Z.; Ehlenberg, D. F.; Qian, Z.; Zhang, S.; Rondeau-Gagné, S.; Phan, M. D.; Ankner, J. F.; Ivanov, I. N.; et al. SMART Transfer Method to Directly Compare the Mechanical Response of Water-Supported and Free-Standing Ultrathin Polymeric Films. *Nat. Commun.* **2021**, *12*, 1–11.
- (26) Matsushige, K.; Radcliffe, S. V.; Baer, E. The Pressure and Temperature Effects on Brittle-to-Ductile Transition in PS and PMMA. *J. Appl. Polym. Sci.* **1976**, *20*, 1853–1866.
- (27) Hoare, J.; Hull, D. The Effect of Temperature on the Deformation and Fracture of Polystyrene. *J. Mater. Sci.* **1975**, *10*, 1861–1870.
- (28) Melick, H. G. H. V.; Govaert, L. E.; Meijer, H. E. H. Localisation Phenomena in Glassy Polymers : Influence of Thermal and Mechanical History. *Polymer* **2003**, *44*, 3579–3591.
- (29) Rabinowitz, S.; Beardmore, P. Craze Formation and Fracture in Glassy Polymers. *Critical Review. Journal of Macromolecular Science*; Taylor and Francis Ltd., 1972; Vol. 1.
- (30) Brown, H. R.; Russell, T. P. Entanglements at Polymer Surfaces and Interfaces. *Macromolecules* **1996**, *29*, 798–800.
- (31) de Gennes, P. G. Glass Transitions in Thin Polymer Films. *Eur. Phys. J. E* **2000**, *2*, 201–205.
- (32) Ediger, M. D.; Forrest, J. A. Dynamics near Free Surfaces and the Glass Transition in Thin Polymer Films: A View to the Future. *Macromolecules* **2014**, *47*, 471–478.
- (33) Liu, Y.; Chen, Y. C.; Hutchens, S.; Lawrence, J.; Emrick, T.; Crosby, A. J. Directly Measuring the Complete Stress-Strain Response of Ultrathin Polymer Films. *Macromolecules* **2015**, *48*, 6534–6540.
- (34) Hasegawa, H.; Ohta, T.; Ito, K.; Yokoyama, H. Stress-Strain Measurement of Ultra-Thin Polystyrene Films: Film Thickness and Molecular Weight Dependence of Crazing Stress. *Polymer* **2017**, *123*, 179–183.
- (35) Zhang, S.; Ocheje, M. U.; Luo, S.; Ehlenberg, D.; Appleby, B.; Weller, D.; Zhou, D.; Rondeau-Gagné, S.; Gu, X. Probing the Viscoelastic Property of Pseudo Free-Standing Conjugated Polymeric Thin Films. *Macromol. Rapid Commun.* **2018**, *39*, 1800092.
- (36) Fetters, L. J.; Lohse, D. J.; Milner, S. T.; Graessley, W. W. Packing Length Influence in Linear Polymer Melts on the Entanglement, Critical, and Reptation Molecular Weights. *Macromolecules* **1999**, *32*, 6847–6851.
- (37) Keddie, J. L.; Jones, R. A. L.; Cory, R. A. Size-Dependent Depression of the Glass Transition Temperature in Polymer Films. *Europhys. Lett.* **1994**, *27*, 59–64.
- (38) Fellers, J. F.; Kee, B. F. Crazing Studies of Polystyrene I. A New Phenomenological Observation. *J. Appl. Polym. Sci.* **1974**, *18*, 2355–2365.
- (39) Yang, A. C.; Kramer, E. J.; Kuo, C. C.; Phoenix, S. L. Craze Fibril Stability and Breakdown in Polystyrene. *Macromolecules* **1986**, *19*, 2010–2019.
- (40) McCormick, H. W.; Brower, F. R. T.; Kin, L. E. O. The Effect of Molecular Weight Distribution on The physical properties of polystyrene. *J. Polym. Sci.* **1959**, *39*, 87–100.
- (41) Sussman, D. M.; Tung, W.; Winey, K. I.; Schweizer, K. S.; Riggleman, R. A. Entanglement Reduction and Anisotropic Chain and Primitive Path Conformations in Polymer Melts under Thin Film and Cylindrical Confinement. *Macromolecules* **2014**, *47*, 6462–6472.
- (42) Baumchen, O.; Fetzer, R.; Jacobs, K. Reduced Interfacial Entanglement Density Affects the Boundary Conditions of Polymer Flow. *Phys. Rev. Lett.* **2009**, *103*, 247801.
- (43) Rathfon, J. M.; Cohn, R. W.; Crosby, A. J.; Rothstein, J. P.; Tew, G. N. Confinement Effects on Chain Entanglement in Free-Standing Polystyrene Ultrathin Films. *Macromolecules* **2011**, *44*, 5436–5442.
- (44) Martin, J.; Krutyeva, M.; Monkenbusch, M.; Arbe, A.; Allgaier, J.; Radulescu, A.; Falus, P.; Maiz, J.; Mijangos, C.; Colmenero, J.; et al. Direct Observation of Confined Single Chain Dynamics by Neutron Scattering. *Phys. Rev. Lett.* **2010**, *104*, 12–15.
- (45) Gao, S.; Koh, Y. P.; Simon, S. L. Calorimetric Glass Transition of Single Polystyrene Ultrathin Films. *Macromolecules* **2013**, *46*, 562–570.
- (46) Forrest, J. A.; Dalnoki-Veress, K.; Stevens, J. R.; Dutcher, J. R. Effect of Free Surfaces on the Glass Transition Temperature of Thin Polymer Films. *Phys. Rev. Lett.* **1996**, *77*, 2002–2005.
- (47) Forrest, J. A.; Dalnoki-Veress, K.; Dutcher, J. R. Interface and Chain Confinement Effects on the Glass Transition Temperature of Thin Polymer Films. *Phys. Rev. E: Stat. Phys., Plasmas, Fluids, Relat. Interdiscip. Top.* **1997**, *56*, 5705–5716.
- (48) Ellison, C. J.; Torkelson, J. M. The Distribution of Glass-Transition Temperatures in Nanoscopically Confined Glass Formers. *Nat. Mater.* **2003**, *2*, 695–700.
- (49) Fakhraai, Z.; Still, T.; Fytas, G.; Ediger, M. D. Structural Variations of an Organic Glassformer Vapor-Deposited. *J. Chem. Phys. Lett.* **2011**, *2*, 423–427.
- (50) Yang, Z.; Fujii, Y.; Lee, F. K.; Lam, C.; Tsui, O. K. C. Glass Transition Dynamics and Surface Layer Mobility in Unentangled Polystyrene Films. *Science* **2010**, *328*, 1676–1679.
- (51) Mattsson, J.; Forrest, J. A.; Börjesson, L. Quantifying Glass Transition Behavior in Ultrathin Free-Standing Polymer Films. *Phys. Rev. E: Stat. Phys., Plasmas, Fluids, Relat. Interdiscip. Top.* **2000**, *62*, 5187–5200.
- (52) Bay, R. K.; Crosby, A. J. Uniaxial Extension of Ultrathin Freestanding Polymer Films. *ACS Macro Lett.* **2019**, *8*, 1080–1085.
- (53) Yiu, P. M.; Yuan, H.; Gu, Q.; Gao, P.; Tsui, O. K. C. Strain Rate and Thickness Dependences of Elastic Modulus of Free-Standing Polymer Nanometer Films. *ACS Macro Lett.* **2020**, *9*, 1521–1526.
- (54) Priestley, R. D.; Cangialosi, D.; Napolitano, S. On the Equivalence between the Thermodynamic and Dynamic Measurements of the Glass Transition in Confined Polymers. *J. Non. Cryst. Solids* **2015**, *407*, 288–295.
- (55) Cangialosi, D.; Alegría, A.; Colmenero, J. Effect of Nanostructure on the Thermal Glass Transition and Physical Aging in Polymer Materials. *Prog. Polym. Sci.* **2016**, *54–55*, 128–147.
- (56) Phys, J. C.; Kremer, K. Erratum: Dynamics of Entangled Polymer Melts: A Molecular-Dynamics Physics. *J. Chem. Phys.* **1991**, *94*, 4103.
- (57) Zhang, T.; Riggleman, R. A. Thickness-Dependent Mechanical Failure in Thin Films of Glassy Polymer Bidisperse Blends. *Macromolecules* **2022**, *55*, 201–209.
- (58) Plimpton, S. Fast Parallel Algorithms for Short-Range Molecular Dynamics. *J. Comput. Phys.* **1995**, *117*, 1–19.
- (59) Towns, J.; Cockerill, T.; Dahan, M.; Foster, I.; Gathier, K.; Grimshaw, A.; Hazelwood, V.; Lathrop, S.; Lifka, D.; Peterson, G. D.; et al. XSEDE: Accelerating Scientific Discovery. *Comput. Sci. Eng.* **2014**, *16*, 62–74.